Conference on Modelling Fluid Flow (CMFF'15)
The 16th International Conference on Fluid Flow Technologies
Budapest, Hungary, September 1-4, 2015

CFD SIMULATION OF A CONNECTED EXPANDER - COMPRESSOR SYSTEM

Péter FÜLE[1], Viktor SZENTE[2]

[1] Corresponding Author. Department of Fluid Mechanics, Budapest University of Technology and Economics. Bertalan Lajos u. 4 – 6, H-1111 Budapest, Hungary. Tel.: +36 1 463 2546, Fax: +36 1 463 3464, E-mail: fule@ara.bme.hu
[2] Department of Fluid Mechanics, Budapest University of Technology and Economics. E-mail: szente@ara.bme.hu

ABSTRACT

In the current study a connected expander – compressor system is investigated. The system is a novel development of such systems to extract mechanical energy from low enthalpy sources, e.g. thermal water, geothermal sources. The system consists of an expander in which warm air expands and flows toward a compressor stage. The connection between the devices has a heat exchanger, thus cooled air is introduced to the compressor. After compression the flow exits the compressor at around atmospheric conditions. During the investigation the Computational Fluid Dynamics (CFD) model of this system is built. The heat exchange in the connecting duct is modelled as an idealised heat exchanger with no pressure loss and perfect efficiency. The aim of the investigation is to find out the flow related parameters and efficiency of the whole connected system with the help of CFD simulations.

Keywords: CFD, low enthalpy heat source, rotary piston compressor, rotary piston expander, thermodynamic cycle

NOMENCLATURE

D_p	[m]	piston diameter
L	[m]	length
M	[Nm]	moment
P	[W]	power
Q	[J]	heat energy
R	[$J/kg/K$]	specific gas constant
S_h	[W/m^3]	energy source term
T	[K]	temperature
V	[m^3]	volume
c_p	[$J/kg/K$]	specific heat capacity
e_0	[J]	total energy
f_{rotor}	[Hz]	rotor frequency
k	[m^2/s^2]	turbulence kinetic energy
m	[kg]	mass
$\dot{m}$	[kg/s]	mass flux
p	[Pa]	pressure
q	[W]	heat flux
s_{out}	[m]	distance to heat exchanger outlet
t	[s]	time
u	[m/s]	velocity
x	[m]	coordinate
δ_{ij}	[-]	Kronecker delta
ε	[m^2/s^3]	turbulence dissipation rate
η	[-]	efficiency
ρ	[kg/m^3]	density
τ_{ij}	[Pa]	viscous stress tensor
ω_{rotor}	[rad/s]	rotor angular velocity

Subscripts and Superscripts

D	desired (temperature at compressor inlet)
c	channel
cell	value at computational cell
current	at current time step
he	heat exchanger
i,j	i-th or j-th component
mech	mechanical
tot	total value for whole system
*	non-dimensional quantity

1. INTRODUCTION

Rotary compressors are widely used in air conditioning systems, cooling systems, e.g. refrigerators [1, 2]. Some advantages of rotary compressors are compact size, low weight, reliability, silent operation, relatively high specific performance and low cost. However these advantages can only be achieved by careful design, optimisation and assembling. [3-5]

There are different ways to separate the low and high pressure chambers of a compressor. The two most common types are spring loaded vane and hinged vane separations. Schematic drawings of these types can be seen in Figure 1. The problem with the spring loaded type is that at high speeds of

revolution the vane can separate from the piston surface due to high acceleration. This leads to temporary leakage and also wears down the components. This problem does not occur with hinged vanes, but the construction becomes more complex. [6]

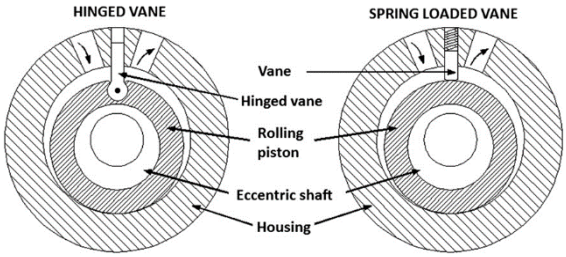

Figure 1. Schematic figure of spring loaded vane and hinged vane type compressors [6]

To avoid the problems mentioned with spring loaded vanes, more solutions are developed. For hinged vane separation there is another special way, when the housing of the compressor is also rotating. This solution is called revolving vane or synchronal rotating compressor. [7-9]

Another method is the sliding vane separation. In this case multiple vanes are mounted in the piston which rotates eccentrically in the housing or concentrically in an oval shaped housing. [10, 11]

Another special solution is the rotating spool compressor, which is similar to the sliding vane concept, but there is only one vane mounted across the whole cross section of the piston. [12, 13]

In the current study the compressor chambers are separated in a way, that the vane is connected mechanically to the driving shaft, this way the connection between the piston and the vane is always ensured. Another difference compared to conventional compressors is that the piston is not rolling along the surface of the compressor chamber's house, but it is solidly mounted on the driving shaft. [14, 15]

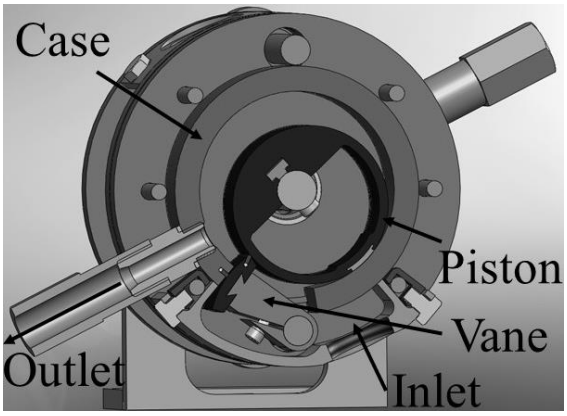

Figure 2. 3 dimensional model of the compressor [14]

Figure 2 shows the assembled model of the compressor showing the most important parts.

The study is focused on a connected system, where the formerly described compressor is connected after an expander (the operation of the compressor is reversed). The point of this concept is to build an inverse engine [14]. Figure 3 shows the schematic drawing of the connected system. The letters "E" and "C" mean expander and compressor respectively. "Q" and "q" describe heat exchange in "H" and "h" heat exchangers. V_f is the feeder valve of the expander and V_o is the outlet valve of the compressor.

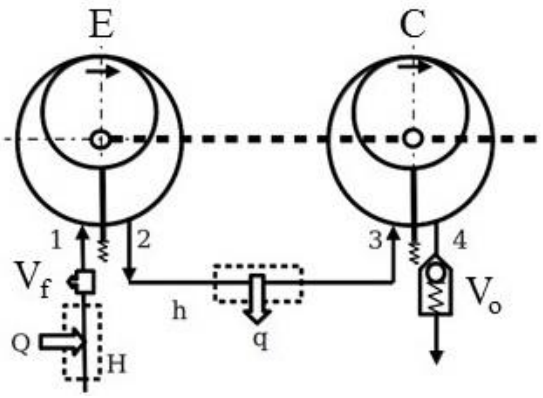

Figure 3. Schematic drawing of the connected expander – compressor system [14]

The expander and the compressor is connected through a heat exchanger which is modelled in the current study as an idealised heat sink.

The working principle is the following: hot air at atmospheric pressure, e.g. from geothermal sources, enters the expander through the feeder valve. As the air fills up the chamber of the expander it performs work on the driving shaft. After closing the feeder valve the air expands as the compressor starts the suction. After a revolution of the piston the air flows through the heat exchanger and it is cooled down to a desired temperature. After that the compressor compresses the cooled air to around atmospheric pressure before it exits to the atmosphere through the output valve. As the air loses heat in the heat exchanger its volume decreases compared to point 1 (assuming equal mass flow rate). Therefore it requires less work to push the air out of the compressor (volumetric and compression work) than the amount it introduced during intake and expansion. This way positive moment can be extracted on the shaft.

The pressure – volume diagram can be seen in Figure 4 and 5 showing the basic thermodynamic processes described above in the expander, exchanger and the compressor. In case of this example – just as for the simulations – the losses are neglected in the system. [14]

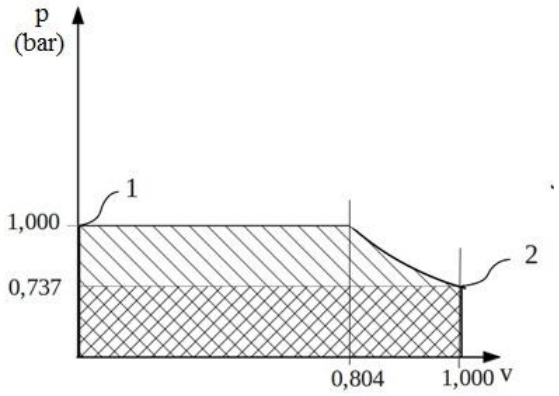

Figure 4. Pressure – volume diagram of expander. Volume is normalised by the maximum chamber volume. [14]

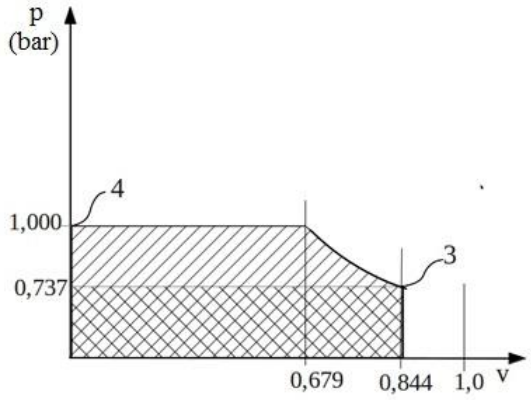

Figure 5. Pressure – volume diagram of compressor. Volume is normalised by the maximum chamber volume. [14]

The system is analysed in various operating states (different rotor frequencies and compressor inlet temperatures) with different connecting channel lengths. The different channel lengths are investigated to find out its impact on the results in order to use as few computational cells as possible. The main goal is to find out the efficiency of the system at various operating conditions.

2. METHODOLOGY

2.1. Governing equations

The simulations are done in ANSYS FLUENT version 14.5. In the simulations the flow is considered compressible and ideal gas law is used. Therefore the governing equations of the flow are the continuity and Navier-Stokes equations for compressible flows, the energy equation and the equation of state of ideal gases (Eqs. (1) to (4)).

$$\frac{\partial \rho}{\partial t} + \frac{\partial}{\partial x_\mathrm{i}}(\rho u_\mathrm{i}) = 0 \tag{1}$$

$$\frac{\partial (\rho u_\mathrm{i})}{\partial t} + \frac{\partial}{\partial x_\mathrm{j}}\left[\rho u_\mathrm{i} u_\mathrm{j} + p\delta_\mathrm{ij} - \tau_\mathrm{ij}\right] = 0 \tag{2}$$

$$\frac{\partial (\rho e_0)}{\partial t} + \frac{\partial}{\partial x_\mathrm{j}}\left[\rho u_\mathrm{j} e_0 + u_\mathrm{j} p + q_\mathrm{j} - u_\mathrm{i}\tau_\mathrm{ij}\right] = 0 \tag{3}$$

$$p = \rho R T \tag{4}$$

The turbulence is modelled by the realizable $k-\varepsilon$ model [16] with enhanced wall treatment.

2.2. Modelling the heat exchanger

One of the goals of the investigation is to model the heat exchanger in the connecting channel between the expander and the compressor. The real life system has a long section of heat exchanger with a relatively complex geometry which would be a long time to model and would take up too many computational cells, thus increasing the computational costs. Therefore simplification of the heat exchanger is needed.

The geometry is simplified to a single channel connecting the expander and the compressor. The geometry can be seen in Figure 6.

This channel has a zone in it, which acts like a heat sink by introducing negative source term into the energy equation. The heat exchanger's fluid dynamic and other losses are neglected, no pressure loss is induced in the current model, but in later models it will be taken into account. The value of the needed source term is computed according to Eqs. (5) to (8) via FLUENT user defined function (UDF). The UDF loops over all cells in the selected zone and calculates the source term value for every cell.

$$Q = c_p m (T_\mathrm{D} - T_\mathrm{cell}) \tag{5}$$

$$t_\mathrm{current} = \frac{s_\mathrm{out}}{u_\mathrm{cell}} \tag{6}$$

$$P = \frac{Q}{t_\mathrm{current}} \tag{7}$$

$$S_\mathrm{h} = \frac{P}{V_\mathrm{cell}} \tag{8}$$

The calculations are based on simple thermodynamic relations. Eq. (5) describes the needed heat energy for a given mass of fluid to achieve the desired temperature, T_D. The mass is computed by the instantaneous density at the current time and the volume of the computational cell. The time needed is approximated by the *x* component of the velocity at the current time and the length in *x* direction to the end of the heat exchanger zone (Eq.

(6)). The cooling (or heating) power is then computed according to Eq. (7). The value of the source term needs to be normalized to unit volume $[W/m^3]$, thus applying Eq. (8) in the end.

It can be seen, that the sign of the source term value depends on the direction of the *x* component of the velocity. To avoid undesirable positive source term values, i.e. heating, for cells with backward flow, the source term value is set to zero for these cells until the *x* velocity becomes positive again.

2.3. Geometry and numerical mesh

The geometry of the connected system can be seen in Figure 6. The compressor is upside down to make the connecting channel as simple as possible. The single straight channel is the least disturbing to the flow and the simplest way to connect the expander and compressor. The results are not influenced by this placement of the compressor, because gravity is not taken into consideration.

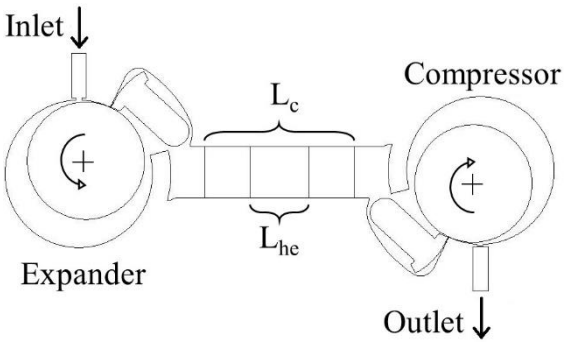

Figure 6. Geometry of the connected system. The channel length is measured from the expander outlet to the compressor inlet.

A non-dimensional channel length, L_c^*, is introduced. It is made non-dimensional by the piston diameter, as seen in Eq. (9).

$$L_c^* = \frac{L_c}{D_p} \tag{9}$$

Three channel lengths are investigated, the base length is $L_c^* = 1.27$, the other two lengths are $L_c^* = 2.54$ and $L_c^* = 3.81$.

The numerical meshes initially contain around 30 000 computational cells depending on the channel length, but this varies as re-meshing is utilized. The pistons are rotating during the simulations and the vanes are also moving with the pistons, thus deforming mesh and re-meshing is used in these zones. These zones are meshed with triangular elements. The non-deforming zones are meshed with quadratic elements. There is a check valve modelled at the outlet section of the compressor. The zone where the valve can move is meshed also with quadratic elements and mesh layering is used. Figure 7 shows the close vicinity of the valve. The two walls which represent the valve can move up and down opening or closing the outlet section. The outlet section is connected to the valve section with mesh interfaces.

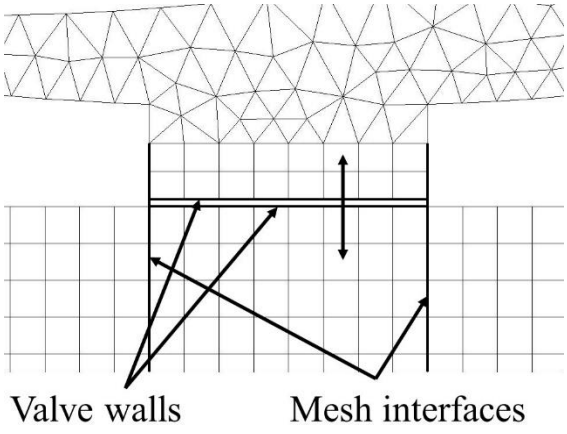

Figure 7. Compressor outlet valve model with the numerical mesh in its vicinity. Triangular cells belong to the compressor's dynamic zone.

In Fig. 7 a part of the triangular mesh of the compressor's dynamic zone can also be seen. The valve walls are moving up and down and the layering process makes sure to insert or collapse cells based on cell size ratios.

2.4. Simulated operating points

Table 1 shows the simulated operating condition values.

Table 1. Simulated operating points

f_{rotor} [Hz]	L_c^* [-]	T_D [K]
20, 30, 50	1.27, 2.54, 3.81	275
20, 30, 50	1.27	293, 303

The impact of the channel length is investigated with $T_D = 275$ [K] and for all the rotor frequencies. Further simulations are carried out only with the shortest channel length, this decision is explained in section 3.1.

The inlet and outlet pressures are set to atmospheric pressure. The inlet temperature is set to 353 [K], the outlet ambient temperature is set to 300 [K].

3. RESULTS

In this section the results are shown from different aspects. First the impact of the channel length is discussed, then the heat exchanger model is analysed and finally the efficiencies are shown.

3.1. Channel length

Table 2 shows the difference in the mean mass flow rate at the inlet between the base channel length and the two longer channels.

Table 2. Inlet mean mass flow rate differences

		L_c^* [−]	
		2.54	**3.81**
$f_{rotor}[Hz]$	**20**	0.8%	3.3%
	30	2.1%	1.8%
	50	2.4%	0.2%

It can be seen that the length of the channel does not influence the inlet mass flow rate significantly. In Table 3 the differences of the total mean moment can be seen. The total mean moment is calculated by summing the mean moment of the expander and the compressor.

Table 3. Total mean moment differences

		L_c^* [−]	
		2.54	**3.81**
$f_{rotor}[Hz]$	**20**	3.1%	5.4%
	30	10.7%	2%
	50	11.8%	4.8%

These differences are somewhat higher than the inlet mean mass flow rate differences, but looking at Figures 8 to 9 it can be said, that the differences are in an acceptable range to say that they do not influence the main trends significantly. Therefore it is sufficient to investigate the further cases with only the shortest channel length saving computational time. Figures 8 to 9 show the inlet mass flow rate and compressor moment for 50 [*Hz*] frequency and the last two simulated revolutions. Aside from the initial transients, the differences in the results are close to within line width, especially for the inlet mean mass flow rate. The characteristics are similar to these on the other two rotor frequencies as Tables 2 to 3 suggest.

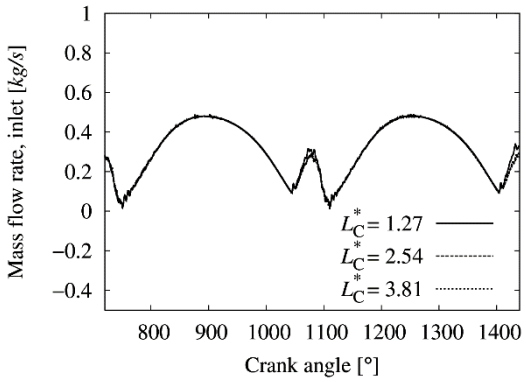

Figure 8. Inlet mass flow rate for the second two revolutions, $f_{rotor} = 50$ [Hz]

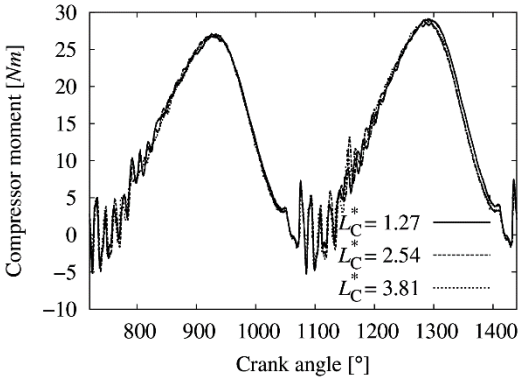

Figure 9. Compressor moment for the second two revolutions, $f_{rotor} = 50$ [Hz]

Also a mesh dependency investigation is carried out with the chosen shortest channel length. The mesh of the compressor and expander is not changed as they are dense enough – based on former experiences [17] – and it would slow down the simulations very significantly, but the mesh of the channel is halved and doubled compared to the base, which has been used before. The mass flow rate and temperature is monitored at the compressor inlet after the channel. These two quantities are important in terms of the heat flux and also can affect the mechanical power - and therefore the efficiency - in the compressor, thus they are chosen for the comparison. The differences compared to the base meshes can be seen in Tables 4 and 5.

Table 4. Mean mass flow rate difference at compressor inlet

		Mesh density	
		half	**double**
$f_{rotor}[Hz]$	**20**	0.1%	2.7%
	30	3.0%	4.9%
	50	0.8%	0.5%

Table 5. Mean temperature difference at compressor inlet

		Mesh density	
		half	**double**
$f_{rotor}[Hz]$	**20**	0.8%	1.3%
	30	0.6%	0.4%
	50	0.1%	0.1%

It can be seen, that the base mesh is appropriate for the preliminary investigations of the system, the differences are under 5% for every case.

3.2. Heat exchanger

The heat exchanger is used in this study to cool the air to a desired temperature before it enters into the compressor. In this study three desired temperature values are tested, namely 275 [*K*], 293

[*K*] and 303 [*K*]. Figures 10 to 12 show the temperature at the compressor inlet for all three frequencies.

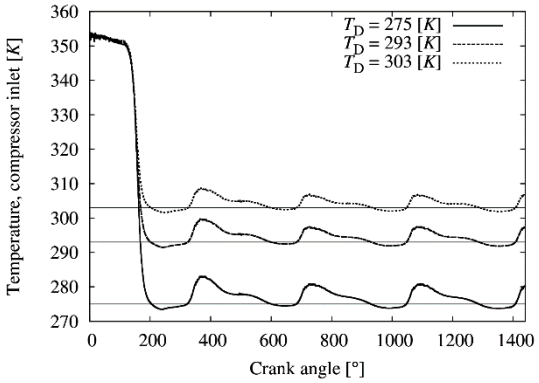

Figure 10. Compressor inlet temperatures for the first four piston revolutions, $f_{\mathrm{rotor}} = 20$ [Hz]

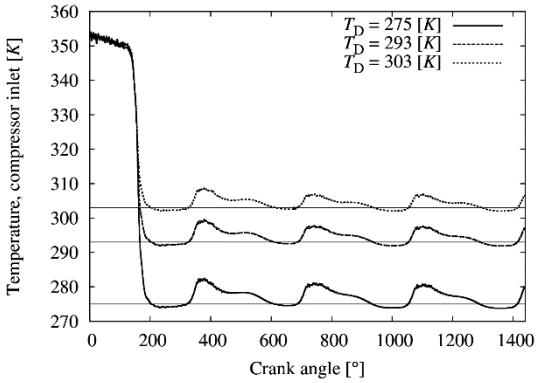

Figure 11. Compressor inlet temperatures for the first four piston revolutions, $f_{\mathrm{rotor}} = 30$ [Hz]

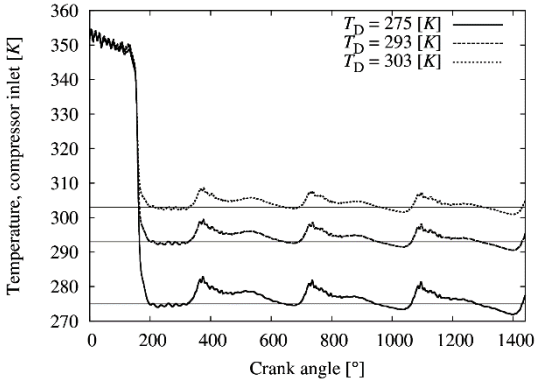

Figure 12. Compressor inlet temperatures for the first four piston revolutions, $f_{\mathrm{rotor}} = 50$ [Hz]

It can be seen, that the heat exchanger model is not able to hold a constant temperature but the results are acceptable, the temperatures alternate around the desired values within an acceptable interval, thus the model can be used for the preliminary studies.

3.3. Efficiency

The efficiency is calculated by mechanical energy and total heat flux. Mechanical energy comes from the total moment of the expander and compressor and the angular velocity (Eq. (10)).

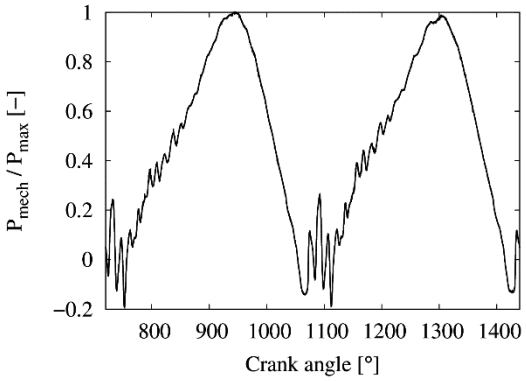

Figure 13. Total power output of expander and compressor, last two simulated revolutions, $f_{rotor} = 50$ [Hz]

In Figure 13 the total power output of the expander and compressor can be seen normalised by the maximum value of the output.

Heat flux is calculated for the expander, heat exchanger and compressor and then it is summed (Eq. (11)). In Figure 14 the heat flux of the heat exchanger can be seen. It is also normalised by its maximum value.

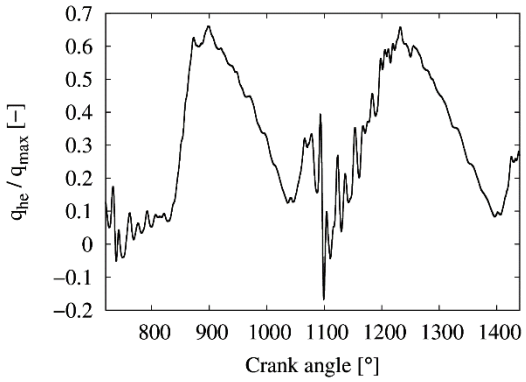

Figure 14. Heat flux of the heat exchanger, last two simulated revolutions, $f_{rotor} = 50$ [Hz]

$$P_{\mathrm{mech}} = M_{\mathrm{tot}}\omega_{\mathrm{rotor}} \tag{10}$$

$$q = c_p \dot{m} \Delta T \tag{11}$$

The ratio of these quantities gives the efficiency of the system (Eq. (12)). First a mean value is calculated for the mechanical power and the heat fluxes, then the ratio can be calculated.

$$\eta = \frac{P_{\text{mech}}}{q_{\text{tot}}} \tag{12}$$

Table 6 shows the calculated efficiencies for the various frequencies and compressor inlet temperatures.

Table 6. Efficiency for various operation points

		$T_{\text{D}}[K]$		
		275	**293**	**303**
$f_{\text{rotor}}[Hz]$	**20**	7%	6.9%	5.2%
	30	9.9%	9.1%	7.7%
	50	19.5%	16.7%	15.8%

It can be seen, that the efficiency is increasing with increasing the rotor frequency and for lower compressor inlet temperatures. From 5.2% the efficiency can go up to almost 20% by increasing the frequency from 20 to 50 [*Hz*] and cooling the compressor inlet air to around 275 [*K*] instead of 303 [*K*]. Referring to [14], where preliminary theoretical calculations can be found for the inverse motor, the obtained efficiency values seem realistic. However these results are obtained by neglecting the heat exchanger's fluid dynamic and other losses and also the losses of the expander and compressor (e.g. leakage losses). By taking this into consideration, the efficiency values will decrease, especially at higher rotor frequencies. The results are to be compared to measurement data in the future.

4. SUMMARY

CFD simulation of a connected expander – compressor system was carried out for various operation points. The system is intended to be used as an inverse motor, extracting energy from low enthalpy heat sources. This work was a preliminary study to identify the effects of certain system characteristics with help of CFD simulations. During the work an idealised heat exchanger was modelled and tested with different temperatures and connecting channel lengths. The simulations showed that the channel length was not impacting the results significantly, thus the shortest channel was sufficient to use, therefore lowering computational costs. The efficiency depending on the operation point parameters was around 5% to 20%. The validation with measurement data and further development of the model is subject of future studies.

ACKNOWLEDGEMENTS

This research has been supported by the New Széchenyi Plan under contract No. KMR_12-1-2012-0199.

REFERENCES

[1] Ooi, K. T., Wong, T., 1997, "A computer simulation of a rotary compressor for household refrigerators", *Applied Thermal Engineering*, Vol. 17, No. 1, pp. 65-78.

[2] Ooi, K. T., 2005, "Design optimization of a rolling piston compressor for refrigerators", *Applied Thermal Engineering*, Vol. 25, No. 5-6, pp. 813-829.

[3] Yanagisawa, T., Shimizu, T., 1985, "Leakage losses with a rolling piston type rotary compressor. I. Radial clearance on the rolling piston", *International Journal of Refrigeration*, Vol. 8, No. 2, pp. 75-84.

[4] Yanagisawa, T., Shimizu, T., 1985, "Leakage losses with a rolling piston type rotary compressor. II. Leakage losses through clearances on rolling piston faces", *International Journal of Refrigeration*, Vol. 8, No. 3, pp. 152-158.

[5] Yanagisawa, T., Shimizu, T., 1985, "Leakage losses with a rolling piston type rotary compressor. III", *International Journal of Refrigeration*, Vol. 8, No. 3, pp. 159-165.

[6] Okur, M., Akmandor, I. S., 2011, "Experimental investigation of hinged and spring loaded rolling piston compressors pertaining to a turbo rotary engine", *Applied Thermal Engineering*, Vol. 31, pp. 1031-1038.

[7] The, Y., Ooi, K. T., 2009, "Experimental study of the Revolving Vane (RV) compressor", *Applied Thermal Engineering*, Vol. 29, pp. 3235-3245.

[8] Yang, H., Qu, Z., Zhou, H., Yu, B., 2011, "Study on leakage via the radial clearance in a novel synchronal rotary refrigeration compressor", *International Journal of Refrigeration*, Vol. 34, No. 1, pp. 84-93.

[9] Tan, K. M., Ooi, K. T., 2011, "Heat transfer in compression chamber of a revolving vane (RV) compressor", *Applied Thermal Engineering*, Vol. 31, pp. 1519-1526.

[10] Bianchi, G., Cipollone, R., 2015, "Theoretical modelling and experimental investigations for the improvement of the mechanical efficiency in sliding vane rotary compressors", *Applied Energy*, Vol. 142, pp. 95-107.

[11] Al-Hawaj, O., "Theoretical modeling of sliding vane compressor with leakage", 2009, *International Journal of Refrigeration*, Vol. 32, pp. 1555-1562.

[12] Kemp, G., Garrett, N., Groll, E., 2008, "Novel Rotary Spool Compressor Design and Preliminary Prototype Performance", *Proceeddings of the International Compressor Engineering Conference*, Purdue University, West Lafayette, IN USA, No. 1328

[13]Kemp, G., Elwood, L., Groll, E., 2010, "Evaluation of a Prototype Rotating Spool Compressor in Liquid Flooded Operation", *Proceeddings of the International Compressor Engineering Conference*, Purdue University, West Lafayette, IN USA, No. 1389

[14]Magai, I., 2014, "http://magaimotor.magai.eu/"

[15]Farkas, B., 2014, "CFD simulation of a new type rolling piston compressor designed for heat pumps", *GÉP*, Vol. 65, No. 5, pp. 37-40.

[16]Shih, T.-H., Liou, W. W., Shabbir, A., Yang, Z., Zhu, J., 1994, "A New $k-\varepsilon$ Eddy Viscosity Model for High Reynolds Number Turbulent Flows – Model Development and Validation", NASA Technical Memorandum

[17]Farkas, B., Szente, V., Suda, J. M., 2015, "A Simplified Modeling Approach for Rolling Piston Compressors", *Period. Polytech. Mech. Eng.*, Vol. 59, No. 2, pp. 94-101.